

Supporting Information

Low Valent Al(II)-Al(II) Catalysts as Highly Active ϵ -caprolactone polymerization catalysts: indication for metal cooperativity through DFT studies

Olga V. Kazarina,^{a,b} Christophe Gourlaouen,^a Lydia Karmazin,^c Alexander G. Morozov,^b Igor L. Fedushkin,^{b*} Samuel Dagorne^{a*}

^aInstitut de Chimie (UMR CNRS 7177)- Université de Strasbourg; 4, rue Blaise Pascal, 67000 Strasbourg, France, Email: dagorne@unistra.fr

^bG.A. Razuvayev Institute of Organometallic Chemistry of Russian Academy of Sciences, Tropinina str. 49, 603950 Nizhny Novgorod, Russian Federation, Email: igorfed@iomc.ras.ru

^c Service de Radiocristallographie, CNRS-Université de Strasbourg, UMR 7177, 1 Rue Blaise Pascal, F-67000 Strasbourg, France

Table of Contents

- NMR data for complexe 3-5 (Figures S1-S5)	pp 2-4
- Summary of crystallographic data for species 3-5 (Table S1)	p 5
- Molecular structure of the Al(II)-CL 4 (Figure S6)	p 6
- ^1H NMR (C_6D_6 , room temperature) monitoring of a 28/1 CL/ 1 mixture (Figure S7)	p 7
- SEC traces of PCL (ROP of CL by a 1000/10/1 CL/BnOH/ 1 mixture) (Figure S8)	p 8
- Plot of M_n vs. CL conversion using 1/BnOH as catalyst (Figure S9)	p 8
- MALDI-TOF of produced PCL (Figure S10)	p 9
- ROP of TMC initiated by species 3-5 with/without BnOH (Table S2)	p 10
- DFT models B , C , $[\mathbf{C}\text{-}\mathbf{D}]^\ddagger$, D , $[\mathbf{D}\text{-}\mathbf{E}]^\ddagger$, E , $[\mathbf{E}\text{-}\mathbf{F}]^\ddagger$, F (Figures S11-S18)	pp 11-13
- DFT-computed Gibbs free energy profile for the reaction of B' with BnOH and CL (Figure S19)	p 14
- DFT models B' , C' , $[\mathbf{C}'\text{-}\mathbf{D}']^\ddagger$ and D' (Figure S20-S23)	pp 15-16

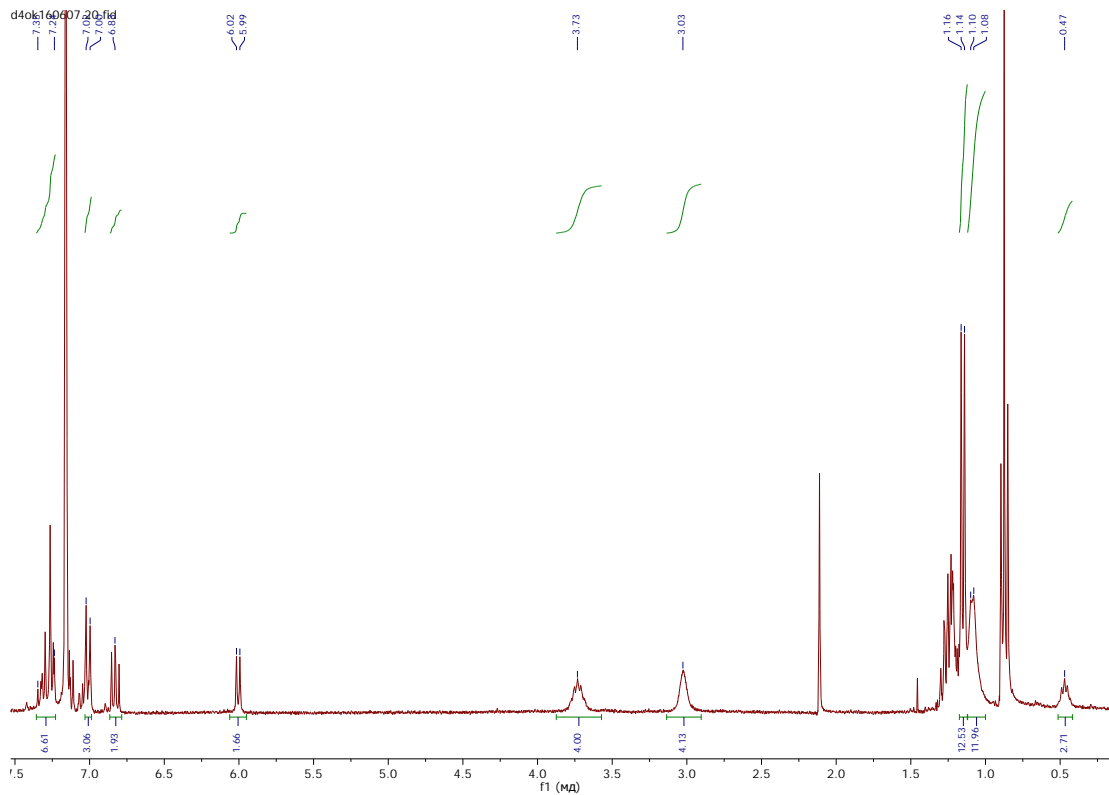


Figure S1. ^1H NMR (C_6D_6) spectrum of the dinuclear Al(II)–TMC adduct **3**.

The low solubility of species **3** precluded the obtainement of exploitable ^{13}C NMR data.

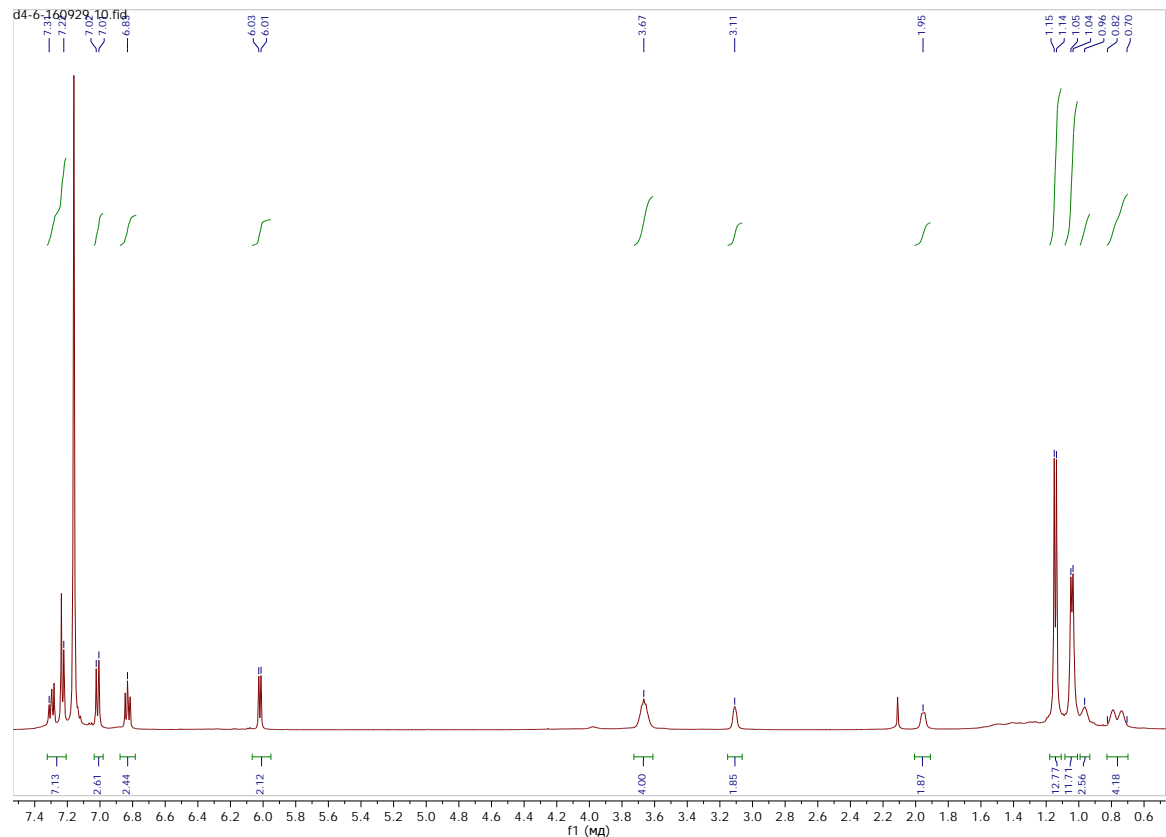


Figure S2. ^1H NMR spectrum of the dinuclear Al(II)–CL adduct **4**.

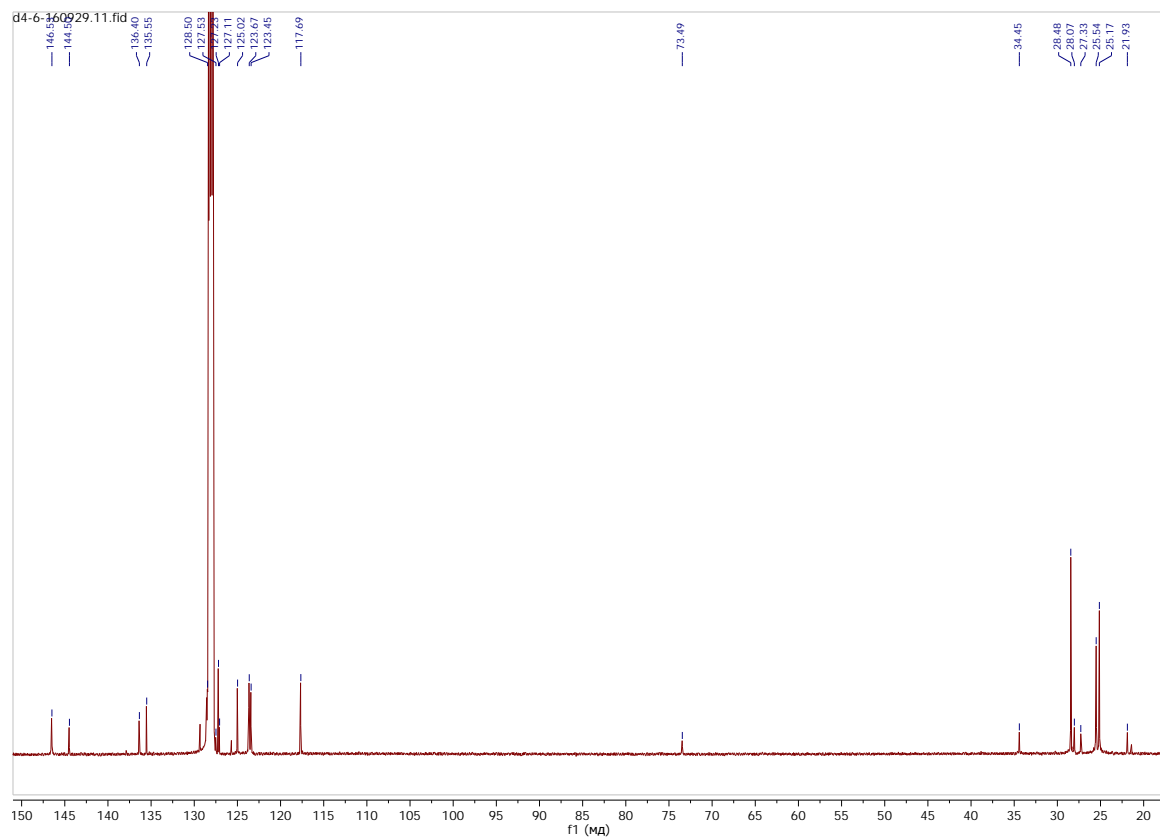


Figure S3. ^{13}C NMR (C_6D_6) spectrum of the dinuclear Al(II)–CL adduct **4**.

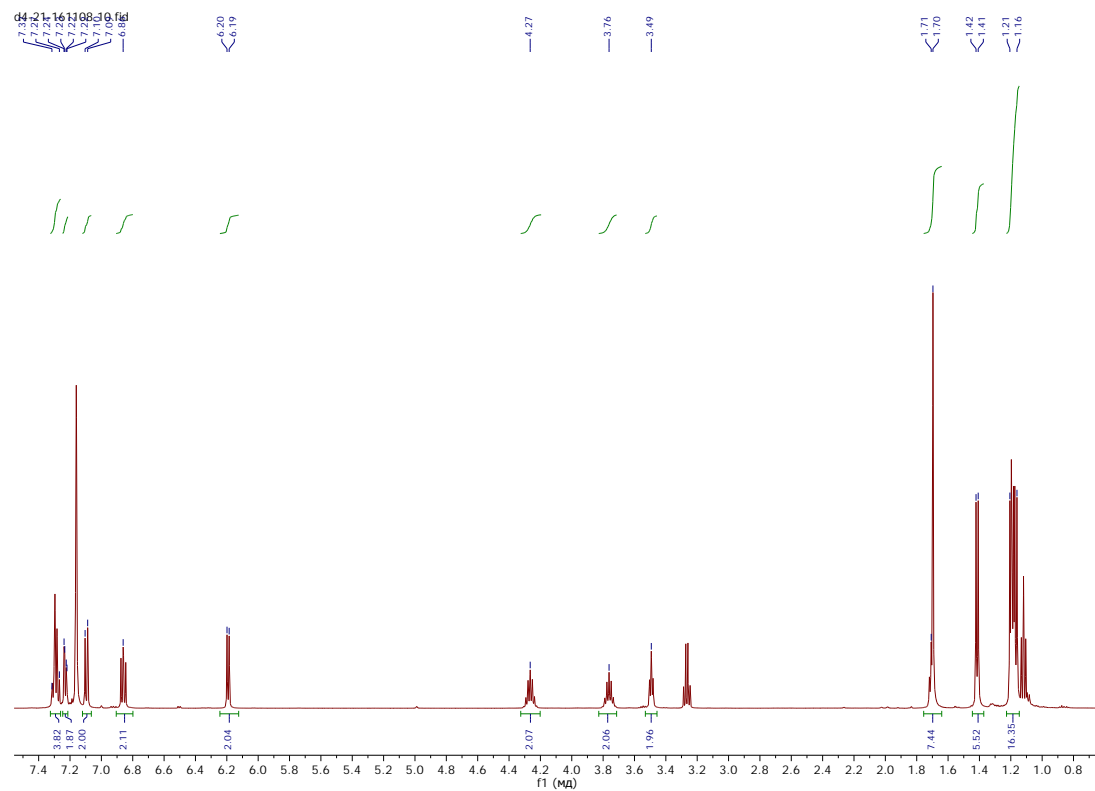


Figure S4. ^1H NMR (C_6D_6) spectrum of species (dpp-bian)Al(κ^2 -{OCH₂CH₂NMe₂}) (**5**)

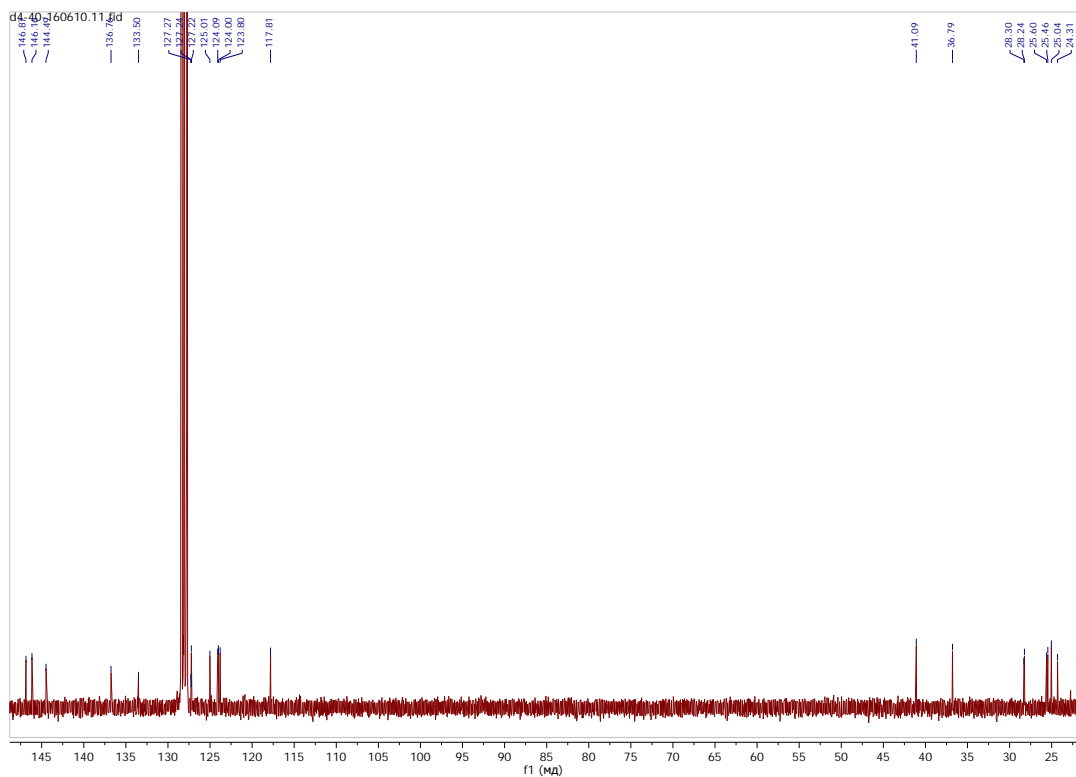


Figure S5. ¹³C NMR (C₆D₆) spectrum of species (dpp-bian)Al(κ^2 -{OCH₂CH₂NMe₂}) (**5**)

Table S1. Summary of crystallographic data for compounds **3** and **5**.

Compound	3	5
CCDC number	1851718	1851716
Formula	C ₈₀ H ₉₂ Al ₂ N ₄ O ₆	C ₄₀ H ₅₀ AlN ₃ O
Molecular weight	1259.53	615.81
Temperature/K	173(2)	173(2)
Wave length/Å	0.71073	0.71073
Crystal system	orthorhombic	monoclinic
Space group	<i>Pccn</i>	<i>P2₁/c</i>
<i>a</i> /Å	20.4001(17)	11.9047(6)
<i>b</i> /Å	23.3701(18)	28.1828(15)
<i>c</i> /Å	16.1214(13)	11.4507(6)
$\alpha/^\circ$	90	90
$\beta/^\circ$	90	95.9530(10)
$\gamma/^\circ$	90	90
<i>V</i> /Å ³	7685.9(11)	3821.1(3)
<i>Z</i>	4	4
<i>d</i> _{calc} /g·cm ⁻³	1.088	1.070
μ /mm ⁻¹	0.089	0.085
<i>F</i> (000)	2696	1328
Crystal size/mm	0.45×0.30×0.15	0.42×0.30×0.15
$\theta_{\min}/\theta_{\max}$	1.325 / 28.042	2.76/28.00
Index ranges	$-26 \leq h \leq 26$ $-30 \leq k \leq 30$ $-21 \leq l \leq 21$	$-9 \leq h \leq 15$ $-37 \leq k \leq 37$ $-15 \leq l \leq 15$
Total reflns	73164	54013
Unique reflns	9305	9241
<i>R</i> _{int}	0.0870	0.0386
Max/min transmission	0.7456 / 0.6716	0.7456 / 0.6511
data/restraints/parameter	9305 / 72 / 450	9241 / 0 / 416
GOF (<i>F</i> ²)	1.074	1.085
Final R indices <i>R</i> ₁ / <i>wR</i> ₂ (<i>I</i> >2σ(<i>I</i>))	<i>R</i> ₁ = 0.0742 <i>wR</i> ₂ = 0.1465	<i>R</i> ₁ = 0.0578 <i>wR</i> ₂ = 0.1251
R indices (all data)	<i>R</i> ₁ = 0.1176 <i>wR</i> ₂ = 0.1653	<i>R</i> ₁ = 0.0792 <i>wR</i> ₂ = 0.1329
Absolute struct. paramet	—	—
Larg. diff. peak/hole (eÅ ⁻³)	0.436 / -0.337	0.325 / -0.338

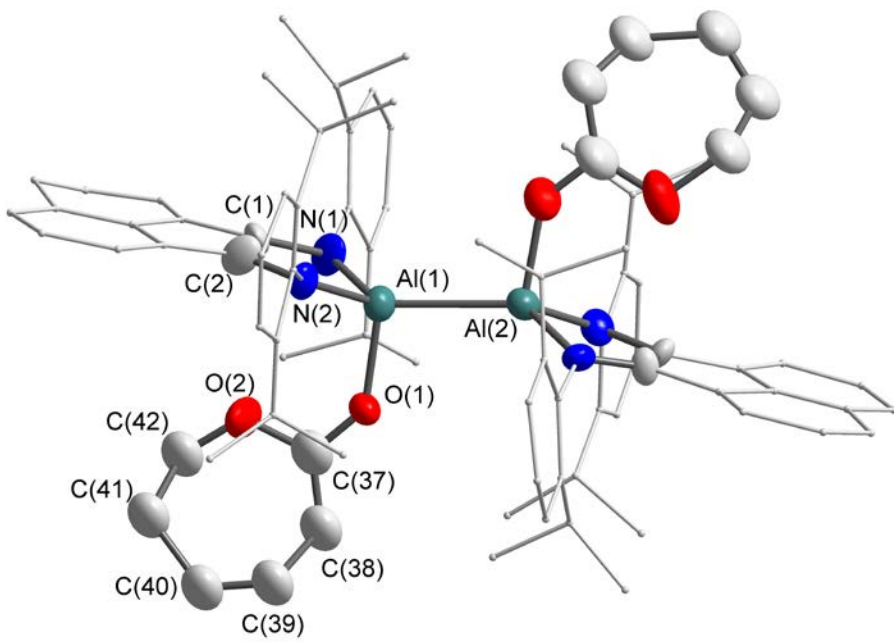


Figure S6. XRD-determined Molecular structure of the dinuclear Al(II)-CL adduct **4**, establishing at atoms connectivity. Poor quality crystals precluded the obtainment of acceptable crystallographic data. Nevertheless, atomic connectivity in **4** could be unambiguously established.

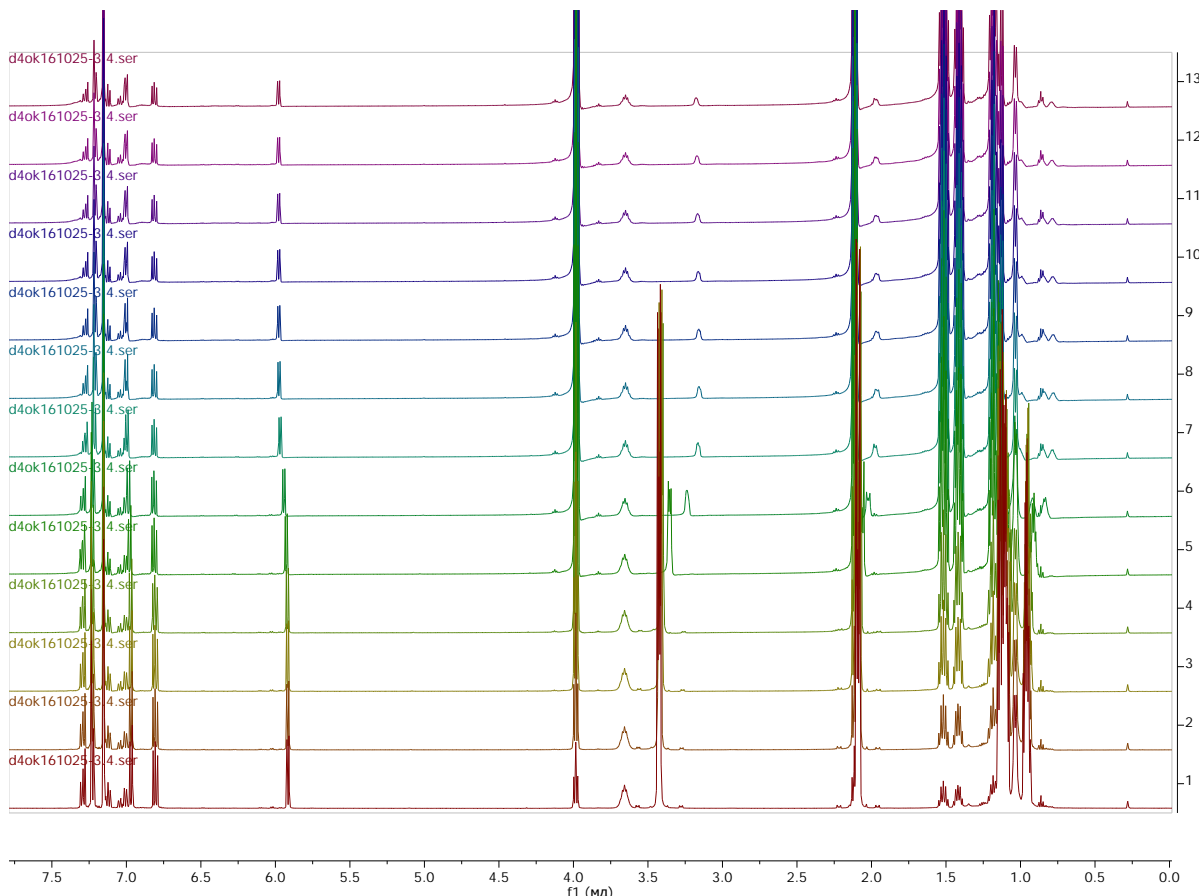


Figure S7. ^1H NMR (C_6D_6 , room temperature) monitoring of a 28/1 CL/**1** mixture. Spectra 1 to 4 are recorded every 15 min till an 1h of reaction time. Spectra 5 to 13 were recorded every hour (after spectrum 4). These data are consistent with the immediate formation of PCL upon mixing CL and **1** (spectrum 1, after 15 min of reaction). The reaction proceeds till complete ROP of CL after 3h (see spectrum 7, with no observable CL monomer) with the concomitant formation of PCL. Regarding the outcome of initiator **1**, spectra 7-13 clearly agree with the quantitative formation of the Al-CL adduct **4**.

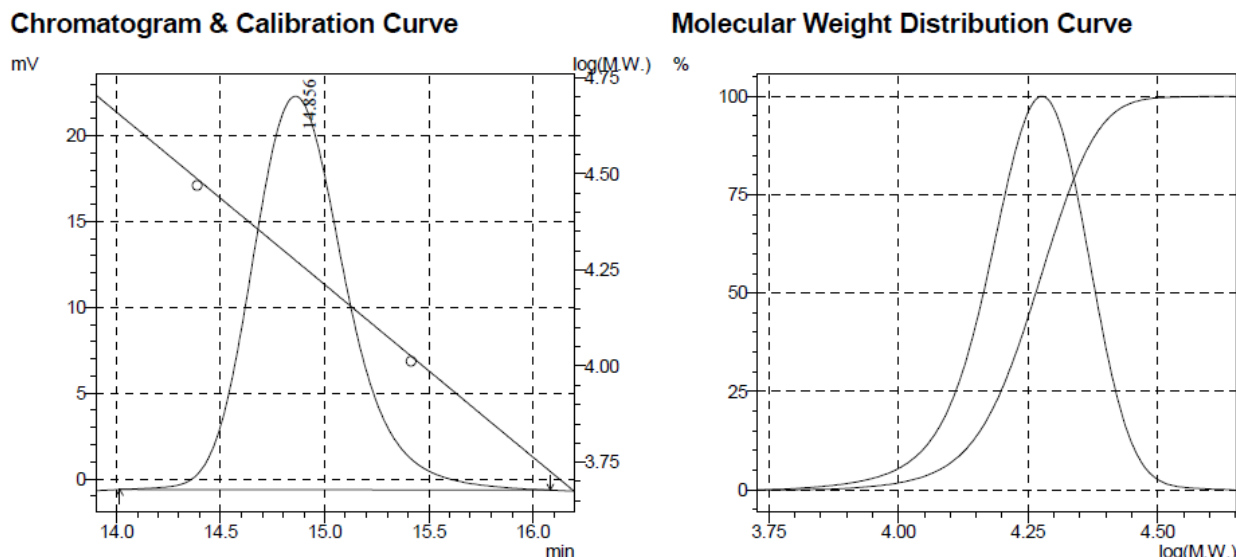


Figure S8. SEC traces of PCL prepared *via* ROP of ϵ -caprolactone initiated by the complex **1**/BnOH. Conditions: 1000 equiv. of CL vs. 10 equiv of BnOH vs. **1**, $[\epsilon\text{-caprolactone}]_0 = 1 \text{ M}$, toluene, rt, 93 % conversion, 15 min).

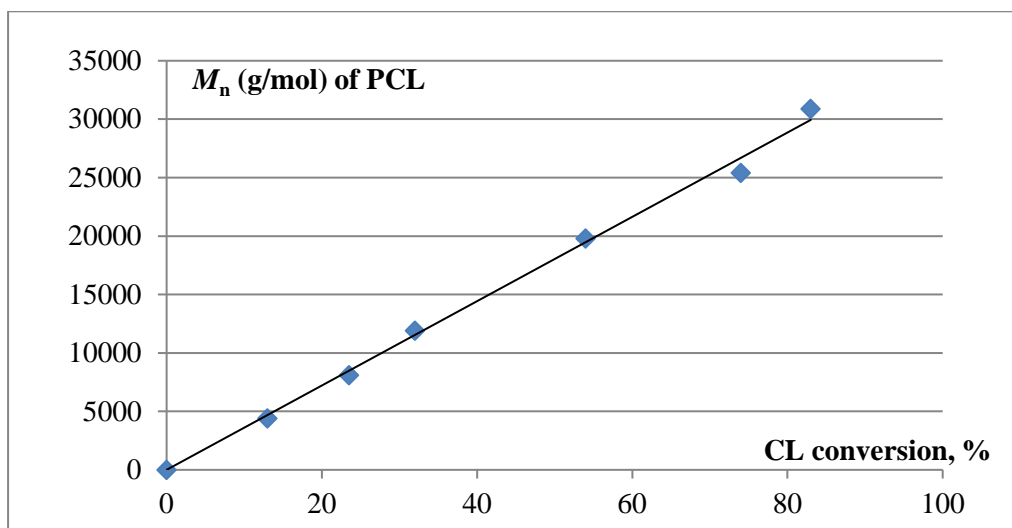


Figure S9. Plot of M_n as a function of the time in the ROP of ϵ -caprolactone using complex **1**/BnOH as catalyst. Conditions: 1000 equiv of CL vs. 3 equiv of BnOH vs **1**, $[\epsilon\text{-caprolactone}]_0 = 1 \text{ M}$, toluene, room temperature.

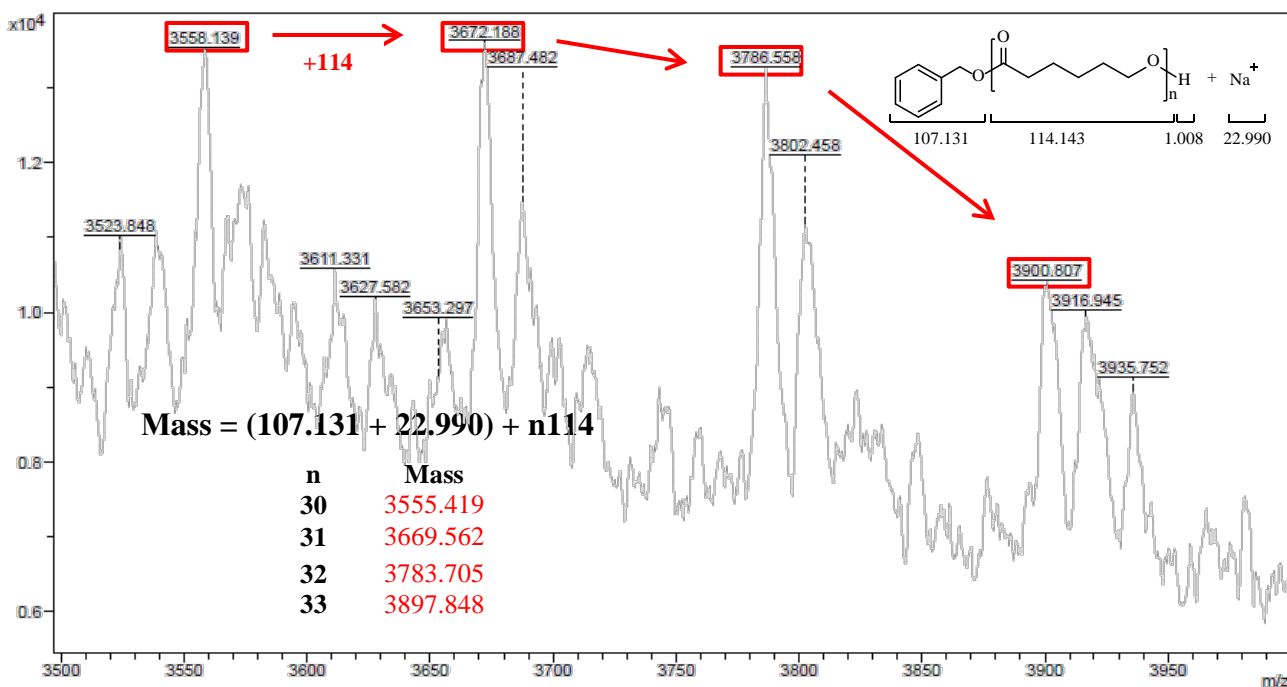


Figure S10. Zoom-in of the MALDI-TOF spectrum of poly- ϵ -caprolactone prepared by ROP of CL initiated using complex **1**/BnOH. Conditions: 1000 equiv. of CL vs. 10 equiv. BnOH vs. **1**, $[CL]_0 = 1$ M, toluene, rt, 93 % conversion, 15 min.

Table S2. ROP of TMC initiated by compounds **3**, **4** and **5** in the absence/presence of BnOH

Nº entry	Cat	TMC ^a	BnOH ^a	time, h ^b	conv. % ^c	M _n , theor ^d	M _n corr ^e	M _w /M _n ^f
1	3	100	-	5	98	9700	48200	3.59
2 ^{g,i}	3	100	1	0.25	97	9900	13000	1.23
3 ^{h,i}	3	1000	10	0.25	15	1500	2800	1.75
4 ^{g,j}	3	100	-	4	81	8200	188300	1.36
5 ^{h,i}	4	100	-	24	22	2300	61100	1.14
6 ^{h,i}	4	100	1	24 ^m	100	10200	18500	1.31
7 ^{h,k}	4	100	-	4	92	9300	505700	1.15
8 ^{h,j}	4	100	-	24	74	7500	159800	1.50
9 ^{h,l}	5	100	-	1	80	8200	42100	1.97

^aAmount in equiv versus catalyst. ^bReaction time. ^cMonomer conversion. ^dCalculated using $M_{n,\text{theor}} = [TMC]_0 / [BnOH \text{ or catalyst}]_0 \times M_{TMC} \times \text{conversion}$. ^eMeasured by GPC in THF (30 °C) using PS standards and corrected by applying the appropriate correcting factor ($M_n < 5000$: 0.57; $5000 < M_n < 10000$: 0.76; $M_n > 10000$: 0.88). ^fMeasured by GPC in THF (30 °C).

^g $[TMC]_0 = 0.5$ M. ^h $[TMC]_0 = 1$ M. ⁱToluene, room temperature. ^jTHF, room temperature.

^kToluene, 80 °C. ^lDichloromethane, room temperature.

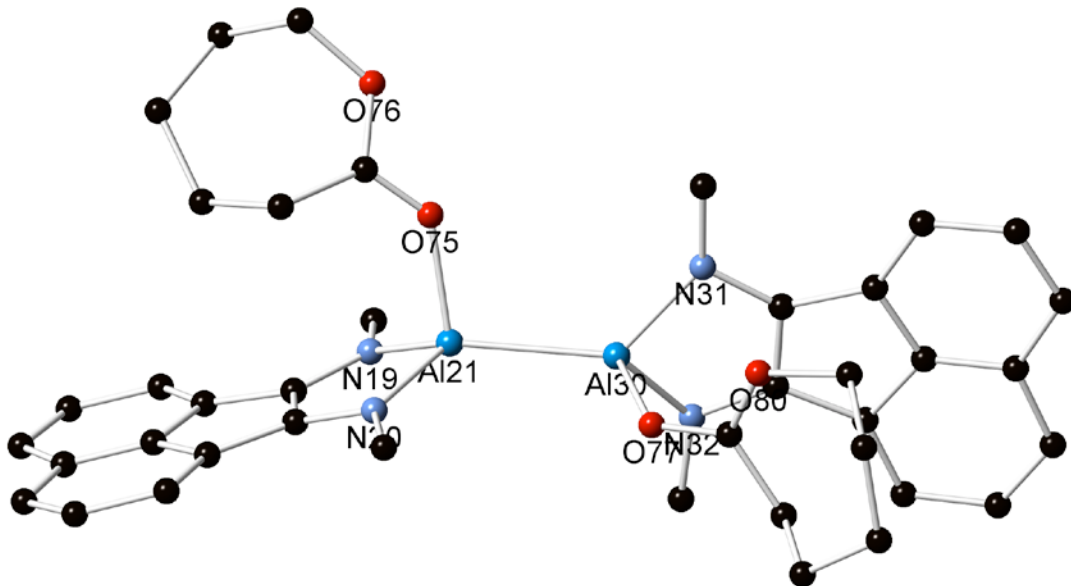


Figure S11. Model adduct $[(\text{Me-bian})\text{Al}(\text{CL})-(\text{CL})\text{Al}(\text{Me-bian})]$ (**B**) arising from the reaction of model $(\text{Me-bian})\text{Al}-\text{Al}(\text{Me-bian})$ (**A**) with 2 equiv of CL.

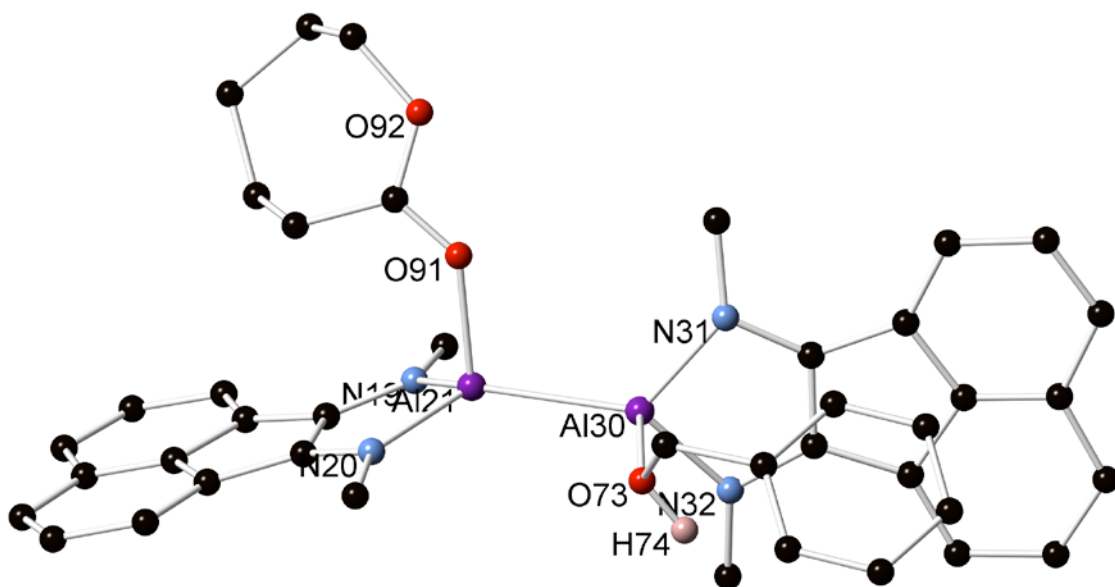


Figure S12. Model adduct $[(\text{Me-bian})\text{Al}(\text{CL})-(\text{BnOH})\text{Al}(\text{Me-bian})]$ (**C**)

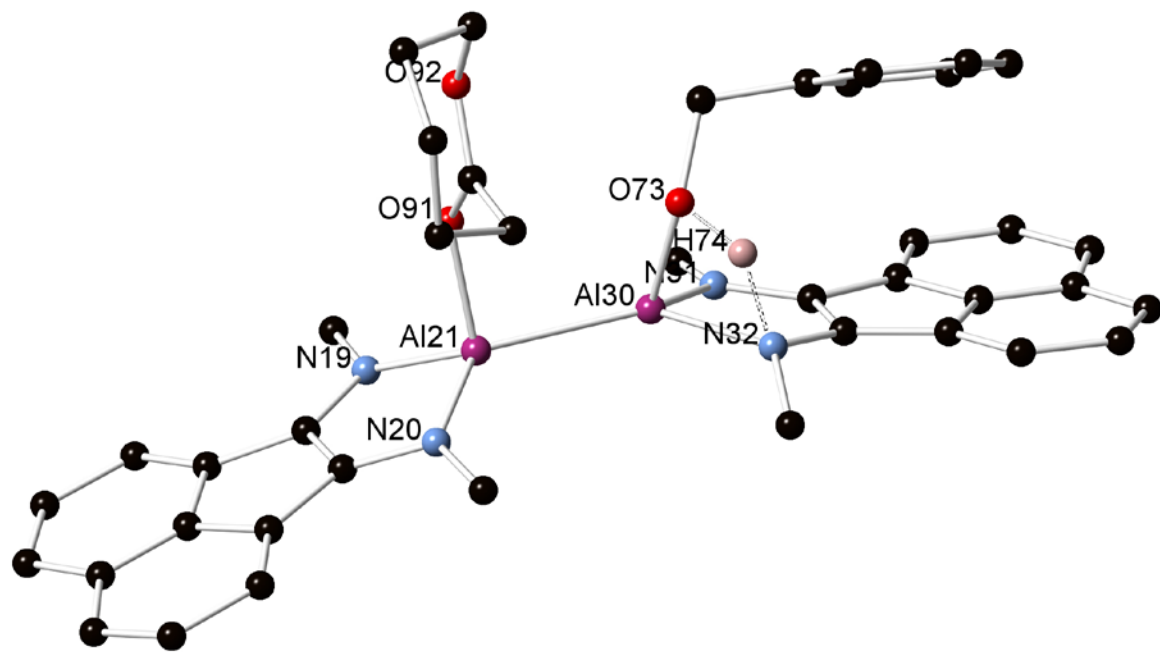


Figure S13. Modeled transition state $[C-D]^{\ddagger}$ allowing the formation of **D** from **C**. Selected distances (\AA): O(73)-H(74) = 1.125, N(32)-H(74) = 1.456.

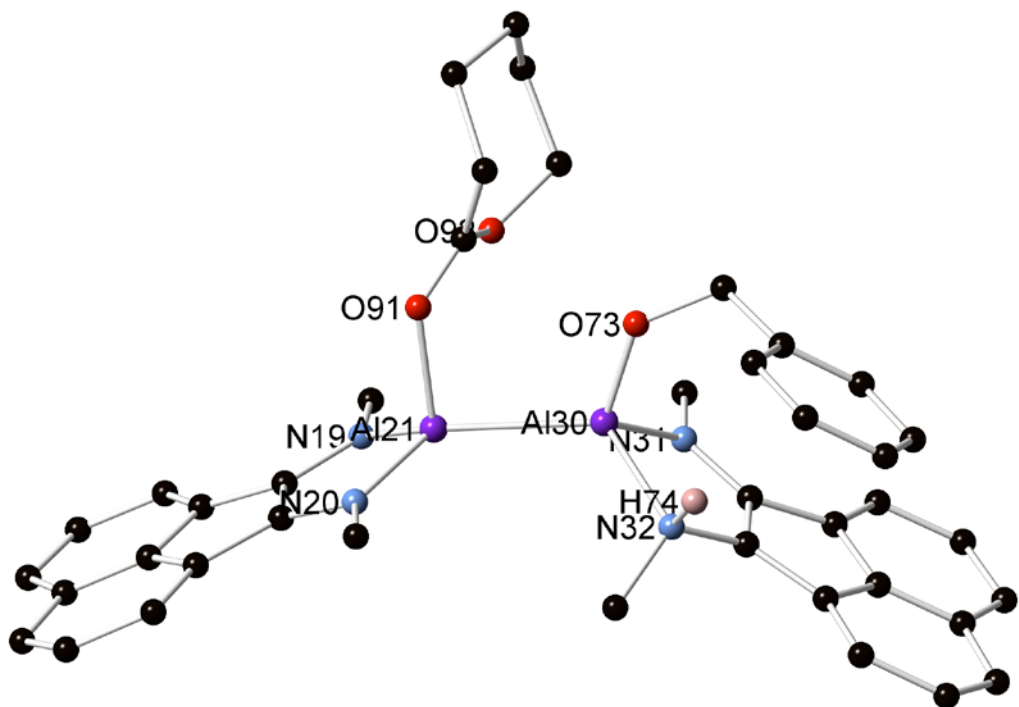


Figure S14. Model adduct $[(\text{Me-bian})\text{Al}(\text{CL})-(\text{BnO})\text{Al}(\text{Me-bian})]$ (**D**) arising from the intramolecular proton transfer reaction of adduct **C**.

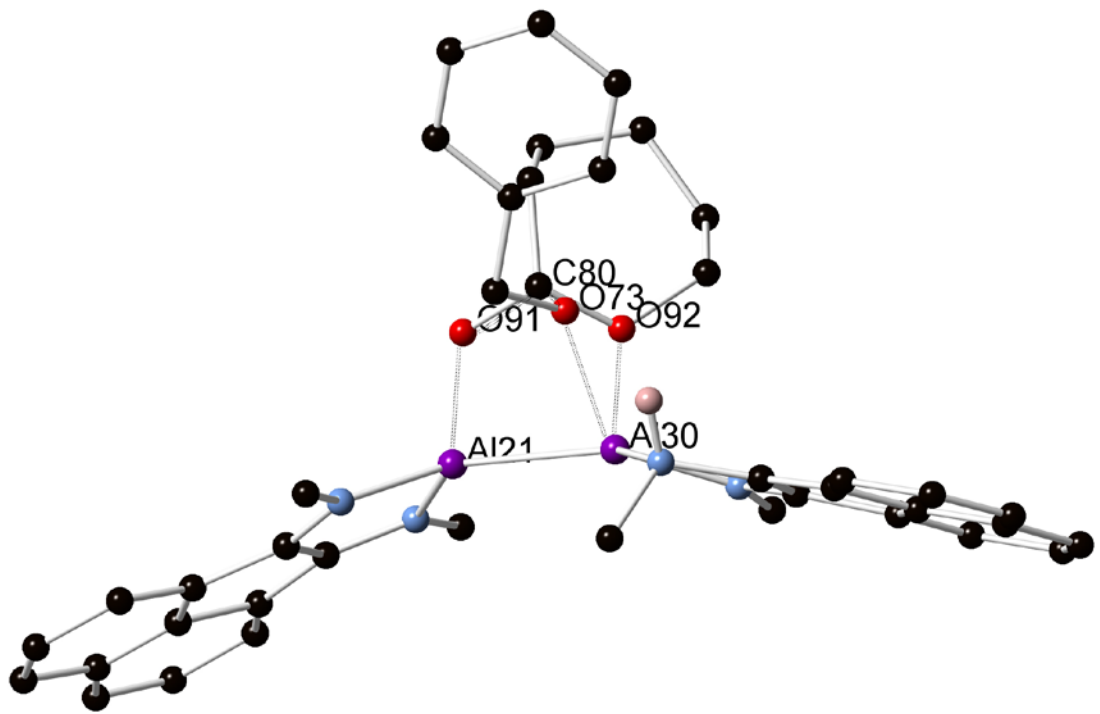


Figure S15. Modeled transition state $[D-E]^{\ddagger}$ allowing the formation of **E** from **D**. Selected distances (\AA): Al(21)-O(91) = 1.885, O(92)-Al(30) = 2.202, C(80)-O(73) = 1.524, C(80)-O(91) = 1.319, Al(30)-O(73) = 2.881.

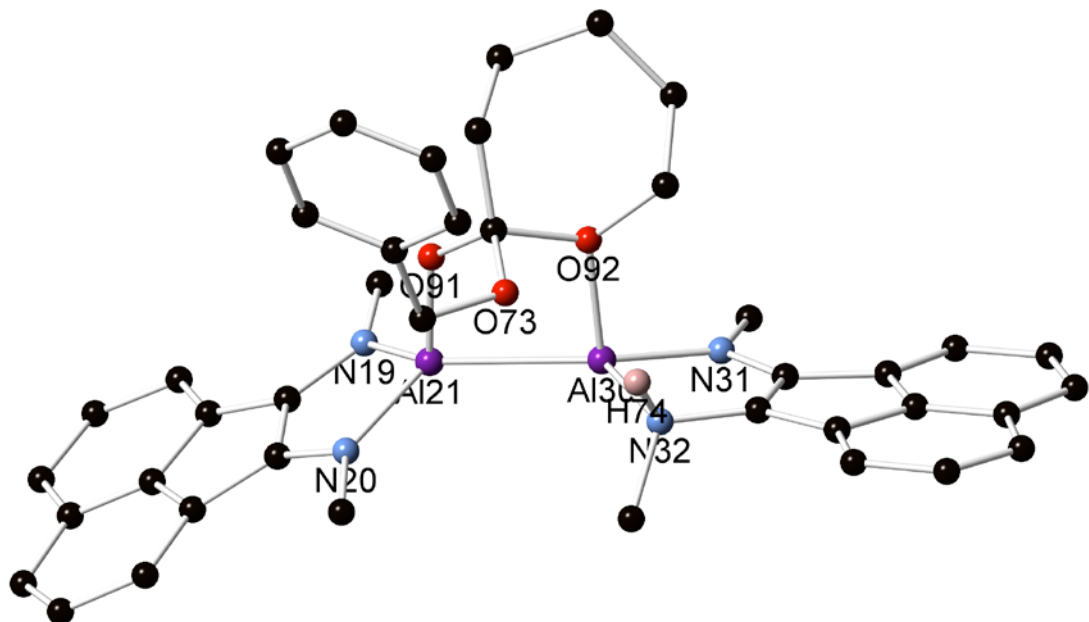


Figure S16. Model adduct **E** arising from the intramolecular nucleophilic attack in model **D**.

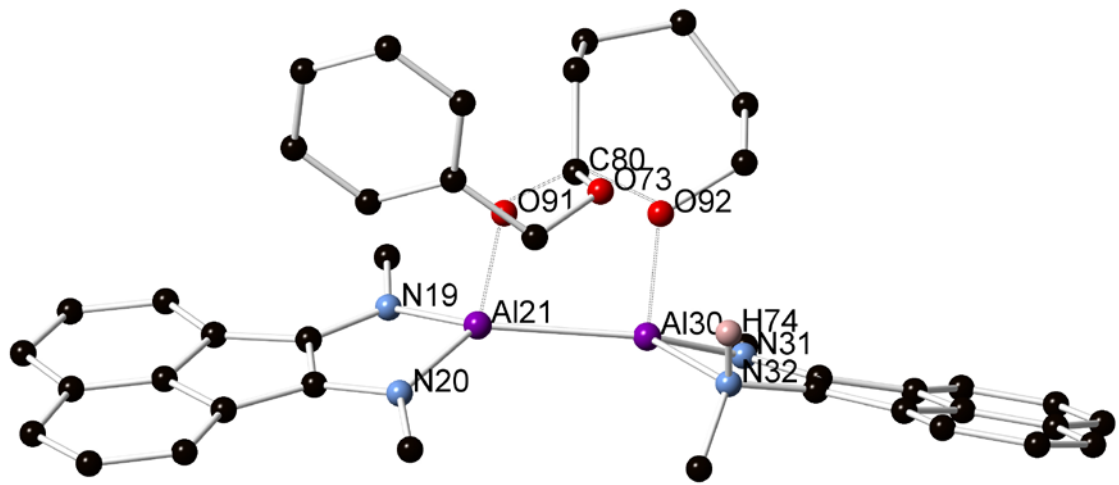


Figure S17. Modeled transition state $[E-F]^{\ddagger}$ allowing the formation of **F** from **E**. Selected distances (\AA): Al(21)-O(91) = 1.858, O(92)-Al(30) = 2.202, C(80)-O(92) = 1.637, C(80)-O(91) = 1.306, Al(30)-O(92) = 1.910.

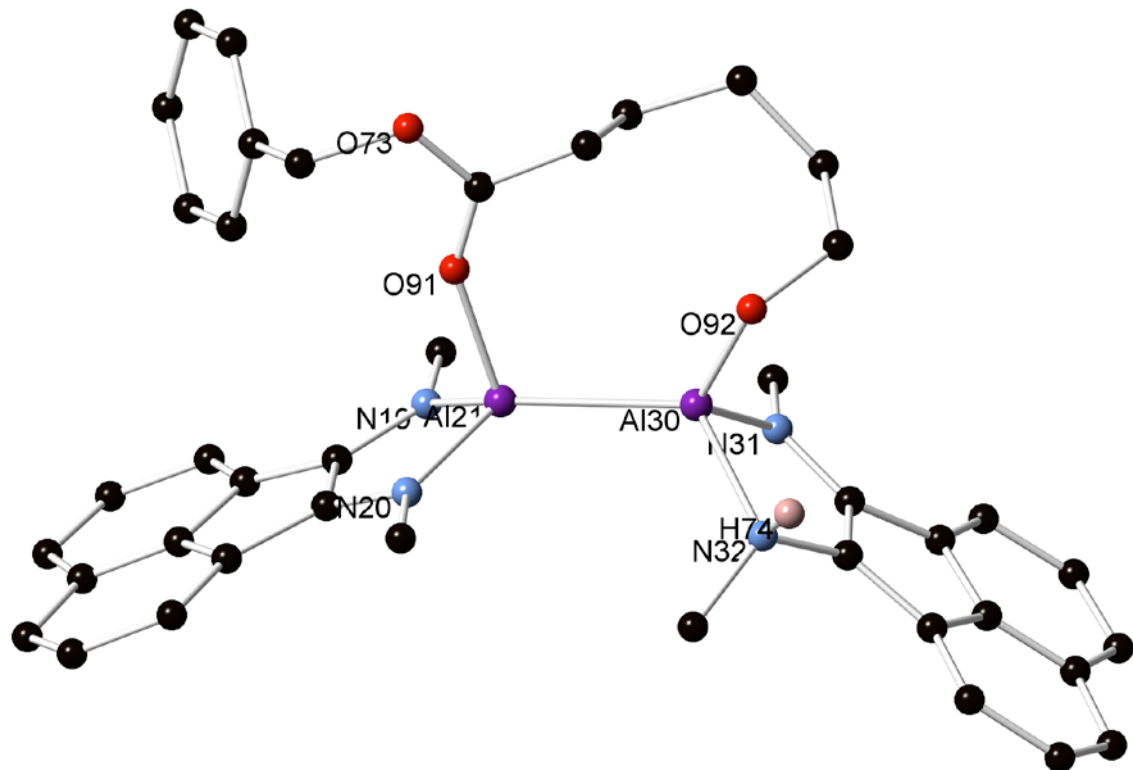


Figure S18. Model adduct **F** arising from the intramolecular ring-opening reaction of model **E**.

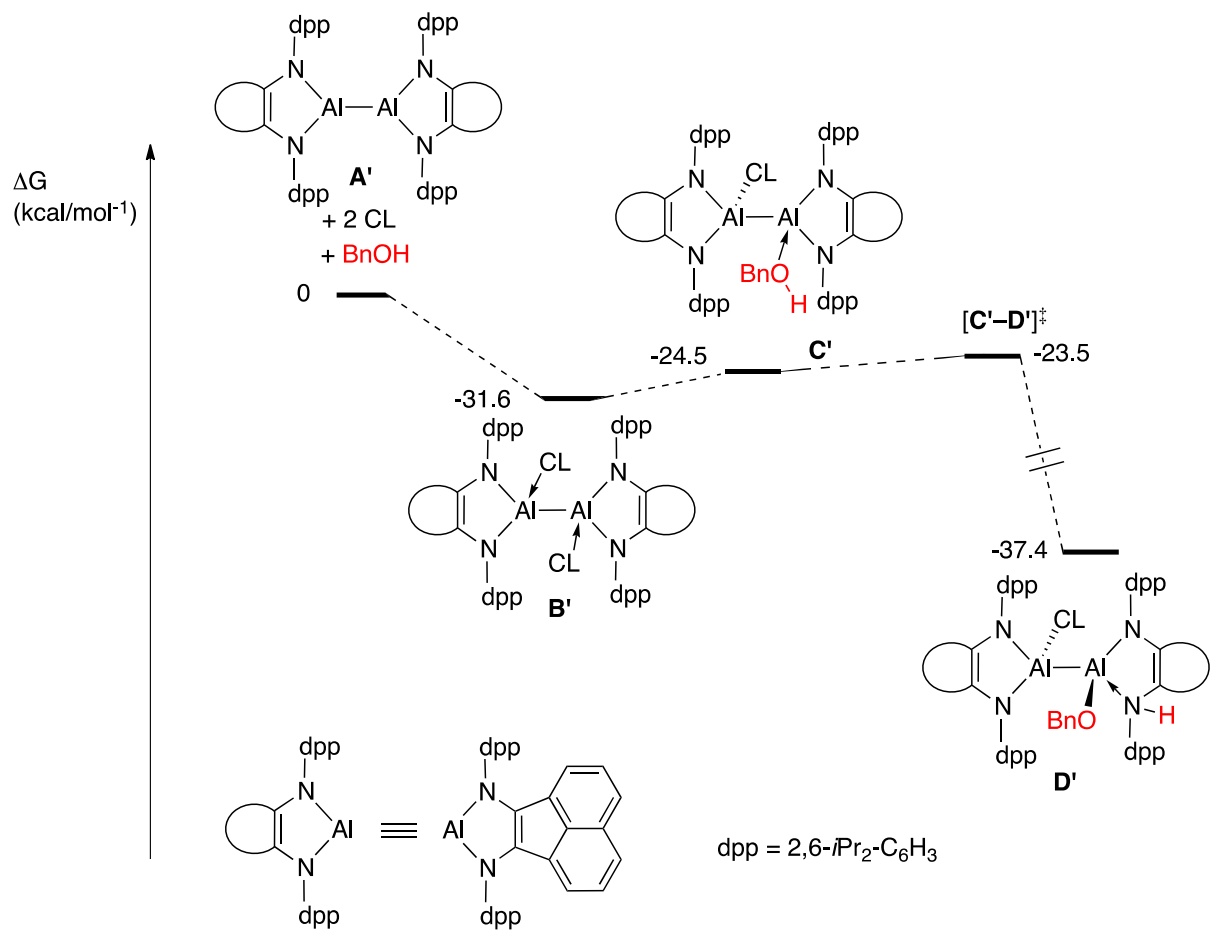


Figure S19. DFT-computed (B3LYP/def2-SVP theory level) Gibbs free energy profile for the initial reaction of **B'**, model compound of species **1**, with CL and BnOH

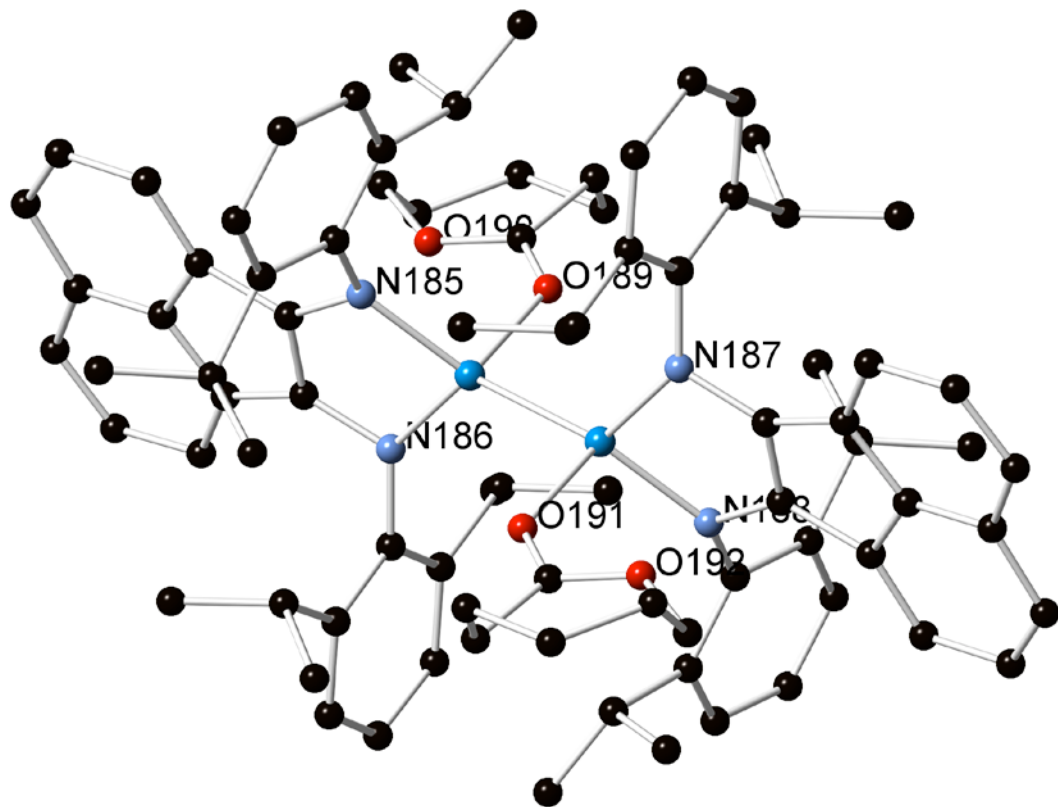


Figure S20. Model adduct $[(\text{dpp-bian})\text{Al}(\text{CL})-(\text{CL})\text{Al}(\text{dpp-bian})]$ (**B'**) arising from the reaction of model $[(\text{dpp-bian})\text{Al}-\text{Al}(\text{dpp-bian})]$ (**A'**) with 2 equiv of CL.

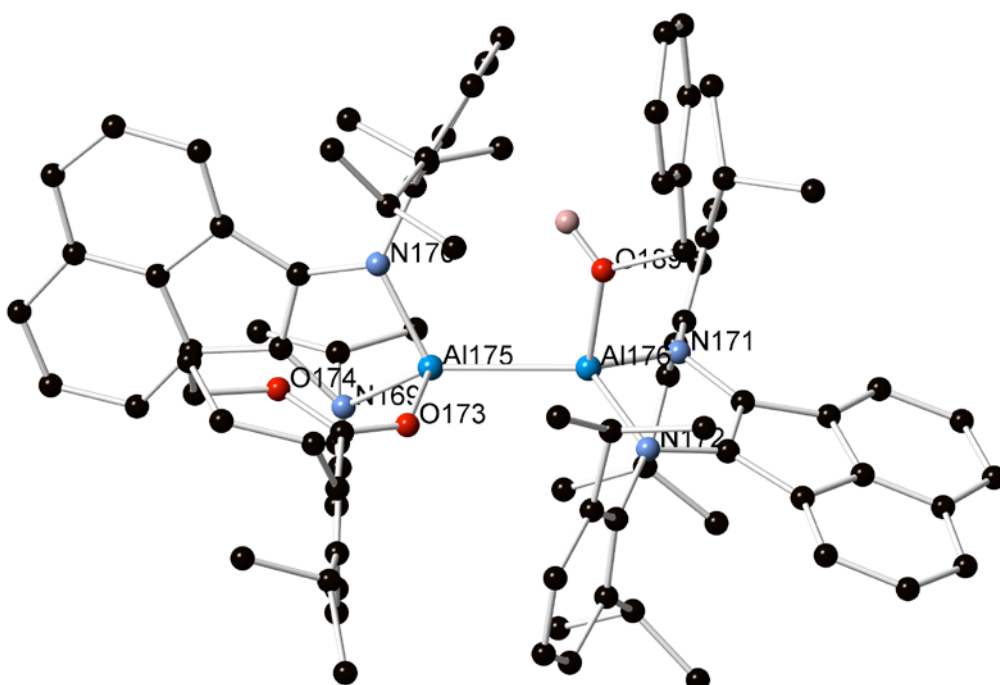


Figure S21. Model adduct $[(\text{dpp-bian})\text{Al}(\text{CL})-(\text{BnOH})\text{Al}(\text{dpp-bian})]$ (**C'**) arising from the reaction of model **B'** with BnOH.

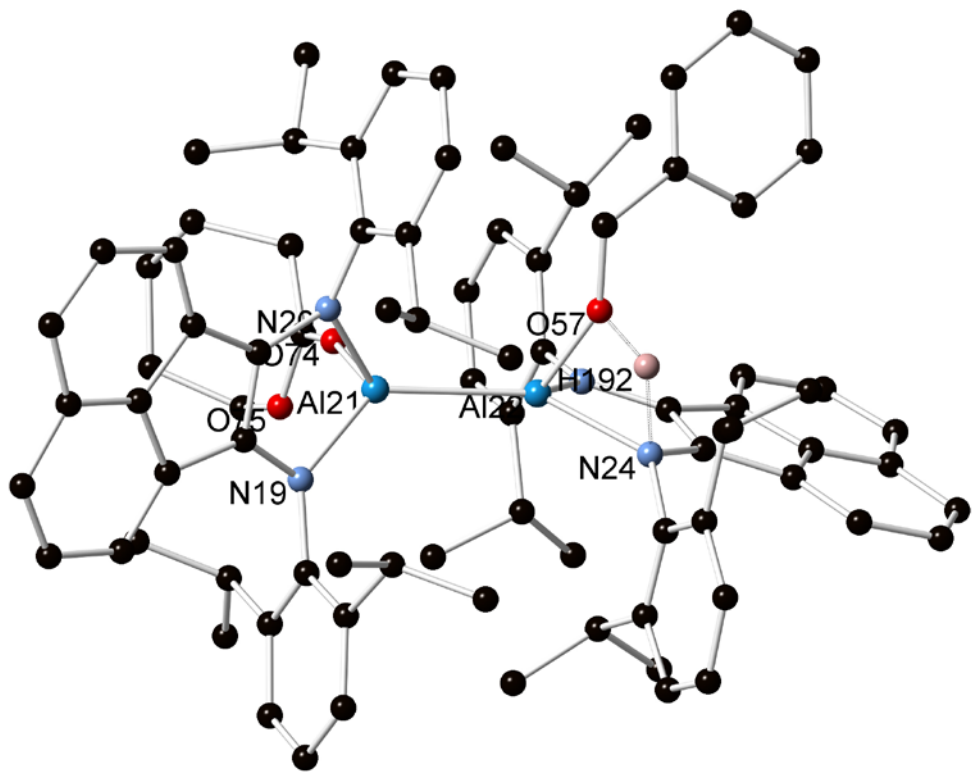


Figure S22. Modeled transition state $[C'-D']^\ddagger$ allowing the formation of **D'** from **C'** via a proton transfer from the Al-BnOH moiety. Selected distances (\AA): O(57)-H(192) = 1.113, H(192)-N(24) = 1.463.

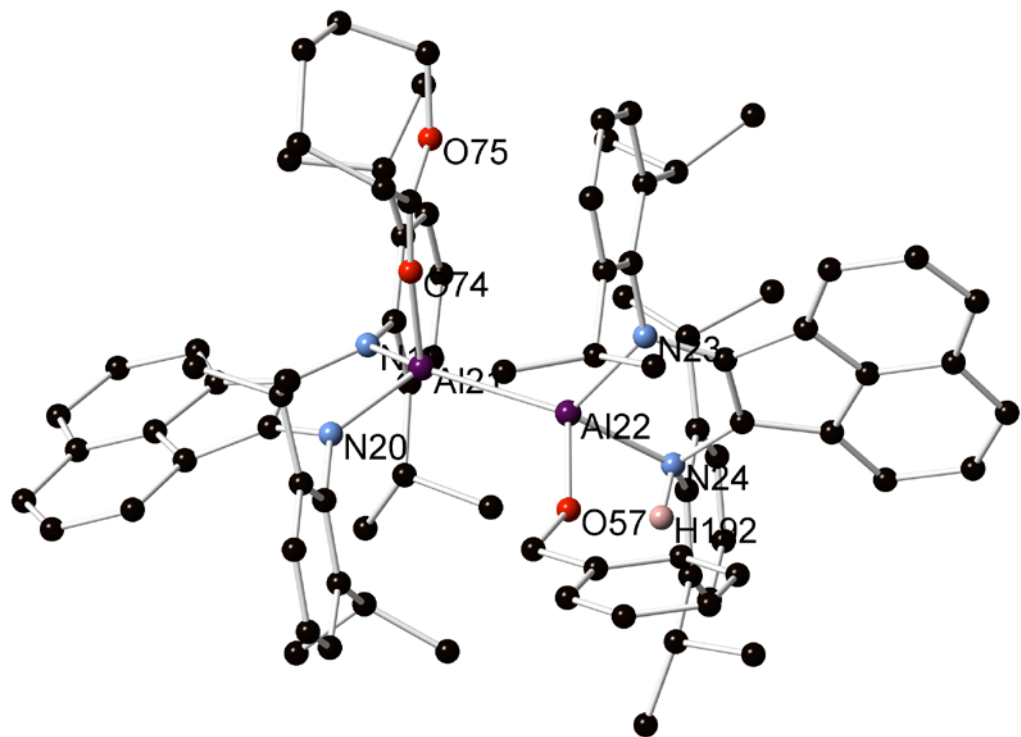


Figure S23. Model adduct **D'** arising from the intramolecular proton transfer of model **C'**.